

Wave-induced sediment resuspension in the Finnish Archipelago, Baltic Sea: ~~Combining small-scale in situ~~ Integrating field measurements and with large-scale numerical model simulations

Jan-Victor Björkqvist¹, Mari Savela^{2,3}, Heidi Pettersson⁴, Victor Alari⁵, and Alf Norkko³

¹Norwegian Meteorological Institute, Allégaten 70, 5007, Bergen, Norway

²City of Helsinki, Työpajankatu 8, 00580 Helsinki, Finland

³Tvärminne Zoological Station, Faculty of Biological and Environmental Sciences, University of Helsinki, J.A. Palméns väg 260, 10900 Hangö, Finland

⁴Finnish Meteorological Institute, P.O. Box 503, 00101, Helsinki, Finland

⁵Department of Marine Systems, Tallinn University of Technology, Akadeemia tee 15a, 12618 Tallinn, Estonia

Correspondence: Jan-Victor Björkqvist (janvb@met.no)

Abstract.

Sediment resuspension, driven by wind-wave-induced shear ~~stresses, plays a crucial role in~~ stress, is a key process influencing coastal water quality, biogeochemical cycles, and the dispersal transport of pollutants and organisms. ~~If the shear stress from waves exceeds an erosion threshold, or~~ The critical shear stress, ~~sediments are resuspended from the seabed. This critical~~ shear stress is an essential τ_{cr} , is a central parameter in sediment transport models, ~~as it determines sediment erodibility since~~ resuspension can occur when wave-induced shear stress exceeds the critical value. In this study, we implemented a high-resolution (20 m) spectral wave model to simulate ~~wave-induced~~ near-bottom orbital velocities across the complex archipelago of southwestern Finland. ~~Near-bottom shear stresses from the model and their respective critical values were estimated using seabed data, with results compared to critical shear stress values obtained through laboratory testing of~~ We then used laboratory measurements from in situ sediment samples. ~~Model data suggested that to determine a model for~~ the critical shear stress ~~could be exceeded over 70 % of the time in certain areas. However, laboratory-determined critical shear stresses were 3–8 times higher than those derived from the model based on median grain size, with modelled shear stresses rarely exceeding the measured critical values. These discrepancies likely stem from unaccounted-for biological and biogeochemical properties of the sediments, which cannot be captured by a simple grain size-based model. We estimate that the accuracy of the wave model~~ data used in this study are of secondary importance compared to the uncertainty of determining the critical shear stress that accounts for physical properties using the median grain size and the dry bulk density, and the time-varying biological variation using chlorophyll *a*. Our proposed model, $\tau_{cr}(d_{50}, \rho_B, ChlA(t))$, explained 66% of the variation of the measured critical stress for our data collected from three different sediment types (Mud, Sand and Mixed sediments). The modelled mean critical shear stress differed between sediment classes were 0.49 N m⁻² for Mud, 1.56 N m⁻² for Sand, and 1.02 N m⁻² for Mixed sediments. The variability in the critical shear stress around the mean values driven by a non-constant biological contribution was approximately 30% for Mud and Sand, and approximately 50% for Mixed sediments. Finally, we used a class-level map of the sea floor and the in situ grain size data to translate the wave model orbital velocities to near-bottom shear stresses. Based

25 on the numerical model data, the critical shear stresses from the newly proposed model, $\tau_{cr}(d_{50}, \rho_B, \text{ChlA}(t))$, were rarely exceeded based on only wave-induced motions in most of the model grid, but could, nonetheless, be exceeded to up around 10% of the times in smaller areas.

Copyright statement. TEXT

1 Introduction

30 Sediment resuspension ~~plays a key role~~ is a key process in shallow coastal environments ~~by~~, influencing water quality, nutrient dynamics, and overall ecosystem health ~~It~~ (Edge et al., 2015; Green and Coco, 2014). Resuspension can release contaminants and nutrients from ~~the sediment~~ sediments, increase turbidity, and redistribute sediment particles, thereby affecting biogeochemical cycles ~~and~~, primary production, ~~altering~~ seabed morphology, and ~~modifying benthic habitat structures~~ benthic habitats (Heiskanen, 1998; Green and Coco, 2014).

35 ~~Sediment resuspension dynamics in coastal areas are primarily governed~~ In coastal areas, resuspension dynamics are primarily driven by wind waves and currents, which exert ~~a~~ shear stress τ (N m^{-2}) on the ~~sediment surface~~. ~~In shallow areas, wave motion is especially influential, as it exerts greater stress on the seabed compared to unidirectional flow, even when instantaneous velocities are similar (Komar and Miller, 1973). Shear stress on the sediment surface mobilizes sediment by dragging and lifting particles, while the gravitational and frictional forces within the sediment resist erosion (Shields, 1936; Soulsby and Whitehouse, 1997). When shear stress on the seabed exceeds the critical shear stress threshold (τ_{cr}), particle motion initiates. This creates the potential for lifting sediment from the seabed it is possible for sediment particles to be lifted~~ into the water column ~~;~~ a process known as resuspension ~~(Shields, 1936; Soulsby and Whitehouse, 1997). In shallow waters where currents are typically weak, wave-induced shear stress is the dominant driver of sediment resuspension (Pascolo et al., 2018).~~

45 ~~The critical shear stress, which determines the potential for sediment resuspension, is influenced by the sediment's physical and biogeochemical properties (Grabowski et al., 2011). Among these, sediment grain size is one of the most fundamental characteristics, as it largely regulates sediment erodibility. Other key properties include e.g. Critical shear stress depends on sediment properties, including grain size, bulk density, water content, clay mineralogy, and organic content. In sandy sediments, critical shear stress is primarily governed by grain size, whereas in finer, muddy and chlorophyll *a* and organic matter content (Grabowski et al., 2011). Grain size is a fundamental determinant of erodibility, but in fine sediments, cohesive forces – caused driven~~ by electrochemical and biological interactions – become increasingly ~~significant (Black et al., 2002; Roberts et al., 1998)~~

50 ~~In addition to physical and geochemical properties, benthic fauna can substantially modify the sedimentary environment through bioturbation, feeding activities, and by altering porosity important (Black et al., 2002; Roberts et al., 1998). Biological factors further modify sediment stability: benthic fauna influence porosity and sediment structure through bioturbation and feeding activities (Mulsow et al., 1998; Michaud et al., 2006; Harris et al., 2015). The influence of macrofauna on sediment~~

stability depends on the organism's size, abundance, morphology, and functioning in and on the sediment (Grabowski et al., 2011; Harris et al., 2011). Furthermore, while vegetation dampens hydrodynamic forces acting on the seabed and stabilizes sediments by binding sediment particles with roots and rhizomes (Madsen et al., 2001). As a result via root systems (Koch et al., 2007; Madsen et al., 2001). Consequently, critical shear stress and resuspension potential can vary considerably in time and space.

The critical shear stress is also a key parameter in vary across space and time (Joensuu et al., 2018, 2020). Although sediment transport models, where it is often estimated based on often estimate critical shear stress from median grain size d_{50} , as illustrated in Hjulström and Postma diagrams (Dade et al., 1992; Grabowski et al., 2011). However, in natural sediments, critical shear stress can vary significantly, increasing (d_{50}) (Dade et al., 1992), natural sediments exhibit substantial variability (Grabowski et al., 2011). Seasonal biofilm formation by microphytobenthos can increase τ_{cr} by up to fourfold in spring and summer due to seasonal dynamics (Le Hir et al., 2007). For example, the succession of microphytobenthos can stabilize sediment surfaces through biofilm formation during spring blooms (Decho, 2000) (Le Hir et al., 2007; Decho, 2000). Despite this complexity, sediment transport models often estimate τ_{cr} solely from median grain size (Dade et al., 1992), ignoring biological and seasonal variability, although a recent modelling study by Zhang et al. (2025) incorporated seasonal values of τ_{cr} .

Our aim in this study is to improve understanding of the discrepancies between modelled and observed sediment erosion and resuspension. Bridging this gap is essential for advancing knowledge of coastal dynamics and ecosystem processes, and the physical and biological forces that influence them. In this study, we compare modelled shear stresses with in situ measurements — an approach that remains uncommon in sediment transport research, where empirical data are often limited or absent.

To accurately predict sediment erosion and resuspension in coastal areas, we need an estimate of the magnitude and variation of the near-bottom shear stress and its critical threshold values. The objectives of this study are To improve predictions of sediment resuspension, we integrate empirical data (Joensuu et al., 2018, 2020) into our modelling approach. Our objectives are: (i) to use high-resolution wave simulation to map the spatial variability of the simulations to map spatial variability in near-bottom shear stresses, stress, (ii) to use the best available spatial seabed model data in combination with in situ samples to estimate median grain size and evaluate corresponding critical shear stresses against laboratory measurements, and develop a spatial and temporal seabed model integrating in situ data to estimate critical shear stress, and (iii) to produce a first estimate of estimate sediment resuspension probabilities based on model data outputs.

Our study area is located in the Hanko archipelago on the northern coast and entrance of the Gulf of Finland, the Baltic Sea (Fig. 1). This region provides an optimal setting for investigating sediment resuspension processes as it is characterized by a mosaic of islands with a diverse range of coastal habitats that capture the spatial variability in seabed composition and encompass the main in the physical and biological factors regulating sediment erodibility and resuspension dynamics.

The Baltic Sea is a semi-enclosed, brackish, and shallow sea, with a mean depth of 54 m and negligible tidal currents. In the study area, bottom currents are generally weak, ranging from a few centimeters per second to a maximum of 10 cm s^{-1} under typical conditions (Westerlund et al., 2018). However, current speed can exceed 10 cm s^{-1} occasionally in narrow channels or during upwelling events (Westerlund et al., 2018; Miettunen, 2024). Consequently, sediment resuspension in this

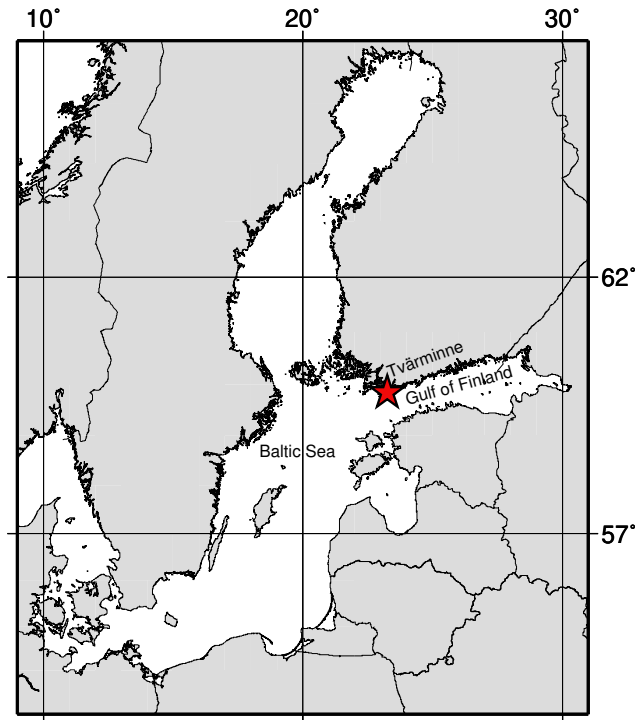


Figure 1. Location of the Tvärminne research station in the western Gulf of Finland, Baltic Sea.

area is predominantly governed by wind-wave induced shear stresses. ~~The prevailing winds in the area are from~~ Prevailing winds are from the southwest, with an average speed of $7\text{--}8\text{ m s}^{-1}$ (Alenius et al., 1998).

90 ~~We simulated the coastal wave conditions using a high-resolution wave model, estimated seabed grain sizes based on publicly available data, and compared our model estimates of median grain sizes and critical stress values with previously gathered field data (??). By quantifying differences between modelled and observed erosion thresholds, this study highlights the importance of incorporating empirical data into sediment transport models. A more accurate understanding of sediment erodibility and resuspension dynamics provides valuable insights for the effective management, conservation, and restoration of coastal zones.~~

95

~~This paper is structured as follows: Section ?? describes the measured and modeled data used in this study, Section 5 presents the modeled estimates of shear stress and compares them to observed values, and Section 6 discusses our findings. Section 7 concludes our findings.~~

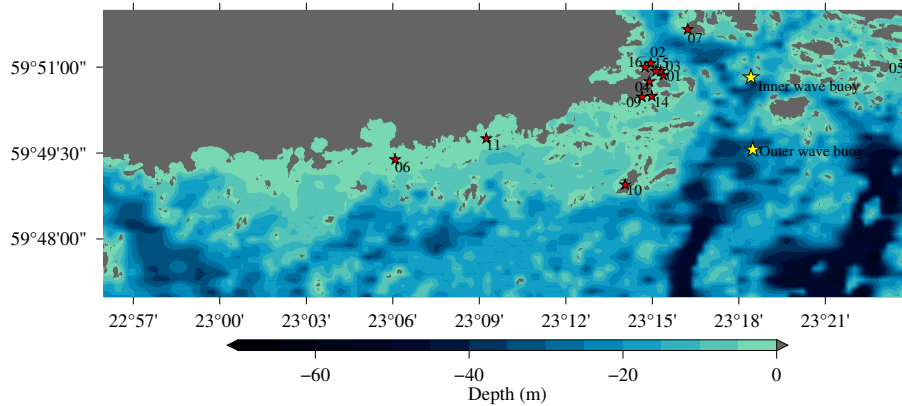


Figure 2. The bottom topography, in situ sediment sampling stations (01–16, marked by red stars), and wave buoy locations (yellow stars) are shown.

2 ~~Materials and Methods~~ Wave data

100 2.1 ~~Measurements~~

2.0.1 ~~Wave buoy data~~

~~Wave observations-~~

2.1 Wave observations

Wave conditions were observed near Tvärminne ~~were available from two locations~~ research station in March and April 2017.
 105 ~~A larger 90 cm Mk-III (?) was moored at approximately 25 meters depth on the outer edge of the Hanko archipelago (Fig. 2, outer wave buoy). A at 24 m depth (outer archipelago) and a smaller 40 cm DWR-G4 Directional Waverider was moored north in the archipelago at a depth of roughly 20 meters (Fig. 2, inner wave buoy) at 17 m depth (inner archipelago) (Datawell, BV, 2025, 2024).~~ Both buoys were located about 3 km east of the Tvärminne research station (Fig. 2).

110 ~~Each wave buoy~~ Both wave buoys sampled at a frequency of 1.28 Hz and calculated the wave spectrum up to 0.58 Hz. Low-frequency data (below 0.05 Hz) ~~)-~~ were discarded when calculating wave parameters.

2.1.1 ~~In situ sediment samples~~

~~Critical shear stress measurements were available from two field campaigns conducted in the years 2014 (?) and 2015 (?) in the Hanko archipelago. In 2014, samples were gathered from 16 shallow sites (depth < 4 m), covering a sedimentary gradient from mud to sand (grain sizes 21 μm–570 μm). These sampling locations are illustrated in Fig. 2. The 2014 field campaign focused on spatial variation in sediment erodibility, maximizing variation in sediment surface characteristics (e.g. bedforms,~~

115

biofilms) across sites. In 2015, three sites (mud (site 4), mixed (site 9), and sandy (site 14) sediment) from the 2014 study were re-sampled from April to December to capture temporal variation in sediment erodibility. In this campaign, variation in sediment characteristics was minimized to focus solely on temporal changes.

120 The sampling procedure was consistent across both campaigns. At each site, SCUBA divers collected samples by carefully inserting EROMES cores (10 diameter, 10 depth) into the sediment. Samples were maintained at in situ temperatures and transported to the laboratory for further measurements. A total of 59 and 73 EROMES cores were collected in 2014 and 2015, respectively. For a detailed description of the sampling procedures, see [?](#) and [?](#) These observations were used to validate the numerical wave model.

125 2.2 Modelled data Wave simulations (SWAN)

2.2.1 Wave simulations

The SWAN model (Booij et al., 1999) is a spectral wave model that was developed especially for shallow water and nearshore simulations. We implemented SWAN for 1 August – 30 September 2014 to catch the spatially extensive sediment measurement campaign ([Joensuu et al., 2018](#)), for 1 May – 30 November 2015 to cover the temporally extensive sediment ~~campaign measurement~~
130 campaign (Joensuu et al., 2020), and 1 March – 30 April 2017 to cover the period of the wave measurements (for validation purposes). Simulations were forced by data from a numerical FMI-HIRLAM weather prediction system (e.g. Eerola, 2013), where the wind speed and direction had been processed to a height of 10 meters. The wind data had a spatial resolution of roughly 7.4 km, and a 1 h temporal resolution for the years 2014 and 2015, and 3 h for 2017.

The model was implemented to a 0.01 nmi (~ 20 m) regular grid with lateral boundary conditions taken from a 1 nmi
135 Baltic Sea wide SWAN simulation using the same wind forcing. A 0.01 nmi resolution is higher ~~that than~~ what is typically used in wave models, but SWAN has been implemented on a similar resolution before in the Baltic Sea (Alari and Raudsepp, 2012). Another spectral model has also been implemented on the North-American coast with an adaptive resolution up to 10 m (Abdolali et al., 2020). The available bathymetric data has been composed of data from nautical charts and the VELMU depth model (<https://ckan.ymparisto.fi/dataset/velmu-syvyyksmalli>) by the Finnish Environment Institute (SYKE) and
140 had a resolution of 0.1 nmi, but the nmi. The land-sea mask has been rasterized based on a polygon dataset from SYKE (<https://ckan.ymparisto.fi/dataset/ranta10-rantaviiva-1-10-000>) and was available at a 0.01 nmi resolution, ~~and land~~. Land points were edited to wet points in the 0.1 nmi bathymetrical grid using the surrounding depth information. Additional depth information from [?Joensuu et al. \(2018\)](#), Valanko (2012), and field sampling were used. The final 0.1 nmi grid was bi-linearly interpolated to a resolution of 0.01 nmi and the land-sea mask was applied (Fig. 2).

145 The wave model produced direct hourly gridded estimates of the maximum near-bottom orbital velocity, U_{bot} (m s^{-1}), and the near-bottom mean periods, $T_{m_{bot}}$ (s). The near-bottom amplitudes, a_{bot} (m), were determined directly by the velocity and period estimates. For a full definition of the wave parameters, see Appendix A.

During the simulation periods, the modelled prevailing wave direction at the outer wave buoy was around 225 degrees, and all waves with a height of 2 m or over came from direction between 175 and 225 degrees. The highest significant wave

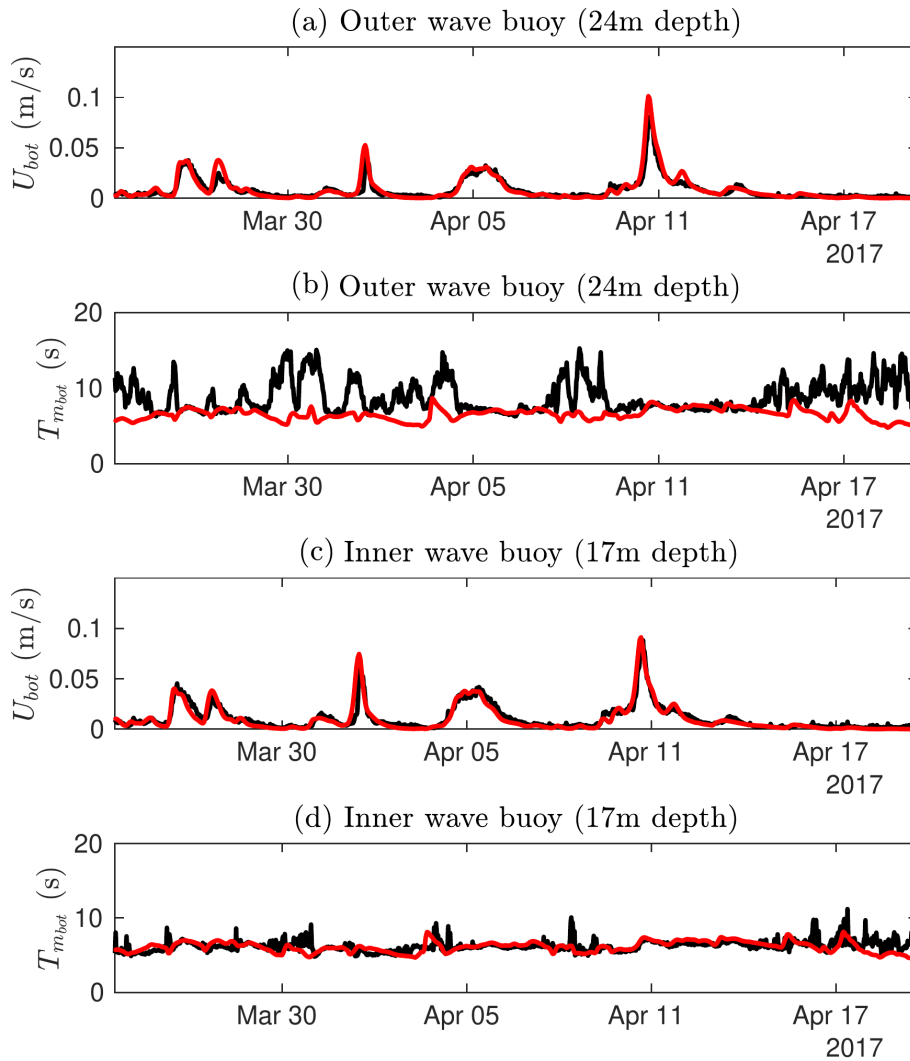


Figure 3. Wave-induced near-bottom orbital velocities and wave period calculated by the SWAN model (red) and the wave spectra measured by wave buoys (black).

150 height of 2.9 m was during a wave event from 195 degrees with mean wave periods (T_{max}) up to 5.8 s. The simulation period also captured high waves (up to 1.7 m) from the east (95 degdeg), although these were less frequent. This distribution aligns with the dominant directions observed in the Gulf of Finland (Pettersson et al., 2010). Statistics of the modelled near-bottom velocities can be found in Appendix B.

We validated the modelled near-bottom orbital velocities and wave periods by determining them from the measured wave
 155 spectrum using the same water depth as in the bathymetrical grid used in SWAN. Near-bottom velocities were **modeled** modelled accurately at both locations (Fig. 3a&c) with the more exposed outer location showing a -0.04 cm s^{-1} bias and

0.47 cm s⁻¹ root-mean-square-error (RMSE). The slightly shallower inner location had a 0.08 cm s⁻¹ bias and 0.49 cm s⁻¹ RMSE. ~~The modeled Modelled near-bottom periods (Fig. 3b&d) were also in good accord with the measurements agreed well at the inner location with a 0.12 s bias and 0.88 s RMSE. For the deeper location the outer location, bias was 2.23 s and RMSE 3.31 s. The clearly worse validation statistics for the outer location is caused by the deeper water depth; the reflecting deeper water where wave orbital motions do not reach the bottom, and the period is determined by low-frequency noise in the measurements. As seen in Fig. 3b, the near-bottom periods were modelled well during the higher near-bottom near-bottom periods were well modelled during high near-bottom velocities, but were less well defined during very less defined under calm conditions. All in all, the Overall, modelled wave data is was sufficiently accurate for this study's purposes.~~

165 2.2.1 Modelled seabed data

~~No direct observations of the seabed type are available at an extent and resolution that could be combined with the wave model data. We therefore based our calculations on data from EMODNET (Seabed Substrates data 1:100k), where the sea floor type has been classified into five categories: Mud to muddy sand, Sand, Coarse sediments, Mixed sediments, and Boulders (Kaskela et al., 2019). An overview of these classifications for the study area is presented in Fig. ??.~~

170 ~~Bottom type classifications from EMODNET data. Corresponding critical shear stresses for representative grain sizes are shown in Table ??.~~

~~The EMODNET dataset does not give representative median grain size (d_{50}) for the five categories. Representative grain sizes for Mud, Sand, and Mixed sediments were determined from in situ measurements. For Coarse sediments and boulders, we used data from the Geological Survey of Finland, which provides minimum, mean, and maximum grain sizes for each class (Kaskela et al., 2019). We used minimum grain size values as representative d_{50} values, given that the mean sizes are exceptionally large. Since finer grains are the first to be mobilized under increasing shear stress, using the minimum grain size provides a more realistic estimate of the threshold conditions for sediment movement. An overview of the chosen representative grain sizes is provided in Table ??.~~

180 ~~Representative grain sizes and corresponding critical shear stresses for each sediment class. Sediment class Grain size (τ_{cr})^a Mud to muddy sand 0.09-0.14 Sand 0.34-0.21 Coarse sediments 2.00-1.20 Mixed sediments 0.15-0.16 Boulders 200.00-178.10~~

2.3 Estimates of seabed shear stress

2.2.1 Modelled shear stresses, τ_w

185 ~~The shear stress values were modelled based on the near-bottom wave induced movements simulated by SWAN, and the estimated grain size (EMODNET).~~

~~The~~

2.3 Wave-induced shear stress, τ_w

The near-bottom shear stress was ~~calculated as~~:

computed as (e.g. Soulsby, 1997):

$$190 \quad \tau_w = 0.5\rho_w f_w U_{bot}^2, \quad (1)$$

where $\rho_w = 1003 \text{ kg m}^{-3}$ is the water density and f_w is a the wave friction coefficient. The friction coefficient was determined following Soulsby (1997) as the higher of the rough and smooth bottom estimates:

$$f_w = \max\{f_{wr}, f_{ws}\}, \quad (2)$$

~~where~~

195 where

$$f_{wr} = 0.237r^{-0.52}, \quad (3)$$

is the rough bottom friction coefficient, $r = a_{bot}/k_s$, $k_s = 2.5d_{50}$ is the Nikuradse equivalent sand grain roughness, and

$$f_{ws} = BR_w^{-N} \quad (4)$$

200 is the smooth bottom friction coefficient. Here $R_w = U_{bot}a_{bot}/\nu$ is the Reynolds number, ν is the kinematic viscosity of water ($1.3 \cdot 10^{-6} \text{ m}^2 \text{ s}^{-1}$, ~~unless given by the in-situ measurement~~), a_{bot} is the amplitude of the wave-induced near-bottom velocities (see Appendix A for a definition), and B and N are constants that depend on the Reynolds number such that:

$$B = 2, N = 0.5 \quad \text{for} \quad R_w \leq 5 \cdot 10^5 \text{ (laminar)}$$

$$B = 0.0521, N = 0.187 \quad \text{for} \quad R_w > 5 \cdot 10^5 \text{ (turbulent)}$$

$$205 \quad \underline{B = 2, N = 0.5 \text{ for } R_w \leq 5 \cdot 10^5 \text{ (laminar)}} \quad (5)$$

$$\underline{B = 0.0521, N = 0.187 \text{ for } R_w > 5 \cdot 10^5 \text{ (turbulent)}} \quad (6)$$

2.3.1 ~~Estimated critical stresses, τ_{cr}~~

~~The critical value of the shear stress is the value that needs to be exceeded in order for resuspension to take place. The critical value depends on the sea floor properties, and is given by~~

$$210 \quad \underline{\tau_{cr} = \theta_{cr}(\rho_s - \rho_w)gd_{50}}$$

3 Environmental data and seabed classification

~~where τ_{cr} ($^{-2}$) is the critical shear stress, θ_{cr} is the threshold Shields parameter, g is the gravitational acceleration (9.82 ^{-2}), ρ_s is particle density (2650~~

3.1 Environmental data

215 Environmental data and critical shear stress measurements were available from two field campaigns conducted in the years
2014 (Joensuu et al., 2018) and 2015 (Joensuu et al., 2020) in the Hanko archipelago. In 2014, samples were gathered from 16
shallow sites (depth < 4 m⁻³), ρ_w is the water density (1003), covering a sedimentary gradient from mud to sand (median
grain sizes 21–570 μm^{-3} , unless given by in situ measurement) and d_{50} is median grain size(). The Shields parameter
(improved by Soulsby and Whitehouse, 1997) can be estimated as

$$220 \theta_{cr} = \frac{0.3}{1 + 1.2D_*} + 0.055[1 - \exp(-0.02D_*)]$$

where D_* is the dimensionless grain size calculated with

$$D_* = \left(\frac{g(\frac{\rho_s}{\rho_w} - 1)}{\nu^2} \right)^{\frac{1}{3}} d_{50}.$$

225). These sampling locations are illustrated in Fig. 2. The 2014 field campaign focused on spatial variation in sediment erodibility,
maximizing variation in sediment surface characteristics (e.g. bedforms, biofilms) across sites. In 2015, three sites (mud (ID04),
mixed (ID09), and sandy (ID14) sediment) from the 2014 study were re-sampled from April to December to capture temporal
variation in sediment erodibility. In this campaign, variation in sediment characteristics was minimized to focus solely on
temporal changes.

3.1.1 Experimental critical stresses, $\hat{\tau}_{cr}$

230 The sampling procedure was consistent across both campaigns. At each site, SCUBA divers collected samples by carefully
inserting EROMES cores (10 cm diameter, 10 cm depth) into the sediment (Schünemann and Kühl, 1991). Samples were
maintained at in situ temperatures and transported to the laboratory for further measurements. A total of 59 and 73 EROMES
cores were collected in 2014 and 2015, respectively. For a detailed description of the sampling procedures, see Joensuu et al. (2018)
and Joensuu et al. (2020). The grain size, dry bulk density and chlorophyll *a* for each measurement site were determined from
the combined 2014 and 2015 data as mean of monthly means (Table 1).

235 3.2 Measurements of critical shear stresses, $\hat{\tau}_{cr}$

In the 2014 and 2015 field campaigns (??)(Joensuu et al., 2018, 2020), the critical shear stresses from the sediment samples
were determined in the laboratory with a portable EROMES device (Schünemann and Kühl, 1991; Andersen, 2001). Bed
shear stress on the sediment surface is generated by turbulent fluctuations induced by a propeller and baffle ring. The baffle
ring prevents rotational flow and ensures turbulent flow fluctuations mimicking those observed by waves in nature. Suspended
240 solids concentration is monitored with an OBS sensor (optical back-scattering sensor). The propeller revolutions have been
calibrated to nominal bed shear stresses (Schünemann and Kühl, 1991; Andersen, 2001).

Table 1. The depth (m), median grain size d_{50} (μm), dry bulk density ρ_B (g cm^{-3}), Chlorophyll *a* ChlA ($\mu\text{g g}^{-1}$) and critical shear stresses, τ_{cr} (N m^{-2}) based on the in situ measurements. $\langle \rangle$ denotes averages, which have been calculated as means of monthly means.

<u>Site</u>	<u>Depth</u>	<u>Type (in situ)</u>	<u>$\langle d_{50} \rangle$</u>	<u>$\langle \rho_B \rangle$</u>	<u>$\langle ChlA \rangle$</u>	<u>$\langle \tau_{cr} \rangle$</u>
ID01	3.9	Mixed sediment	158	1.90	14.00	0.78
ID02	3.2	Sand	320	1.97	16.97	1.12
ID03	3.0	Mixed sediment	155	1.90	16.38	1.12
ID04	2.3	Mud	55	1.44	19.95	0.54
ID05	2.6	Sand	502	1.77	22.52	0.45
ID06	3.0	Sand	216	1.90	9.95	0.80
ID07	3.0	Sand	419	1.95	19.18	0.79
ID09	3.0	Mixed sediment	154	1.76	21.68	0.96
ID10	3.8	Sand	370	2.00	19.70	-
ID11	3.2	Sand	389	2.00	6.35	0.81
ID14	3.4	Sand	274	1.92	27.34	1.52
ID15	3.7	Mixed sediment	178	1.82	13.65	0.48
ID16	3.5	Mud	78	1.50	17.88	0.45

At each run, the bed shear stress was increased every 2 min by 0.1 N m^{-2} from 0 to 2.0 N m^{-2} in the year 2014 study and from 0 to 1.6 N m^{-2} in the year 2015 study. Water samples for gravimetric analysis were collected during each run to calibrate the OBS sensor into suspended solids concentration (SSC; mg l^{-1}) (Andersen, 2001; Andersen and Pejrup, 2002).
 245 The critical shear stress (N m^{-2}) was defined at the erosion rate of $0.1 \text{ (g m}^{-2}\text{s}^{-1})$, which describes the erosion after the erosion of unconsolidated "fluffy" material (Andersen, 2001; Andersen et al., 2005). For a more extensive description of the laboratory procedures, see [Joensuu et al. \(2018, 2020\)](#).

4 Results

Since the EROMES device is not reliable for large grain sizes, we excluded individual critical stress measurements when the
 250 median grain size of the sample exceeded $300 \mu\text{m}$. Consequently, no reliable measurements were obtained from site ID10 (Table 1).

3.1 Model estimates of shear stresses Class-based seabed model

We used EMODnet Seabed Substrates (1:100k) (Kaskela et al., 2019) to define seabed classes: Mud to muddy sand, Sand, Mixed sediments, Coarse sediments, and Boulders (see Fig. 4a). Coarse sediments and Boulders were excluded from this
 255 study, since we had no in situ data from those seabed types. For Mud, Sand, and Mixed sediments we determined representative

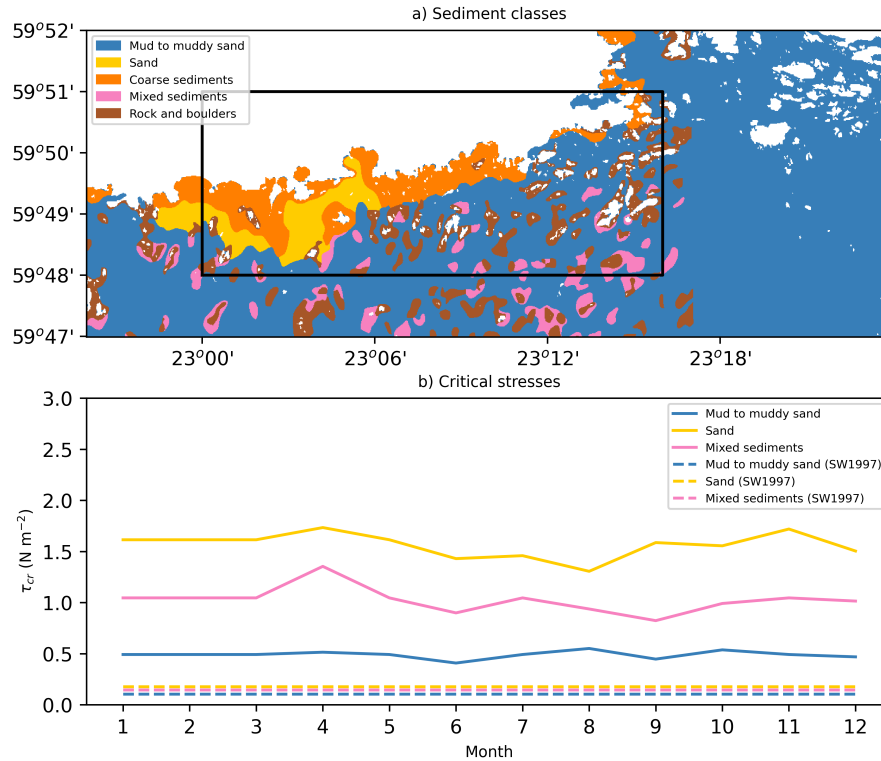


Figure 4. The sediment classes from the EMODnet data (a) and the critical shear stresses estimated based on the time varying model (Eq. 10) and the d_{50} model of Soulsby and Whitehouse (1997) (Eq. 7) (b). The black rectangle in (a) is the area shown in Figures 6–9.

median grain sizes for each seabed type based on the data from Sect. 3.1 (Table 2). The representative values were determined as means of monthly means to not give too much weight to data from the spatial campaign.

The modelled shear stresses were estimated based on the near bottom velocities, and the friction coefficients that were derived from the near bottom wave parameters and the estimated grain sizes

260 4 Models for critical shear stresses, τ_{cr}

4.1 Soulsby and Whitehouse (1997)

The critical value of the shear stress is the value that needs to be exceeded in order for resuspension to take place. The critical value depends on the sea floor properties, and is given by

$$\tau_{cr} = \theta_{cr}(\rho_s - \rho_w)gd_{50} \quad (7)$$

Table 2. Representative physical properties for each sediment class used in the model. The values for chlorophyll *a* is an average outside the growth season (growth season marked in bold), and is used if there is no month-specific value available.

Variable	Mud	Sand	Mixed sediments
d_{50} (μm)	59	284	169
ρ_B (g cm^{-3})	1.45	1.92	1.83
ChlA ($\mu\text{g/g}$)	19.48	29.58	21.57
January	~	~	~
February	~	~	~
March	~	~	~
April	20.28	33.83	32.55
May	~	~	~
June	16.50	23.01	16.35
July	~	24.05	~
August	21.58	18.60	17.71
September	17.88	28.60	13.65
October	21.10	27.48	19.63
November	~	33.32	~
December	18.66	25.66	20.46

265 where τ_{cr} (N m^{-2}) is the critical shear stress, θ_{cr} is the threshold Shields parameter, g is the gravitational acceleration (9.82 m s^{-2}), ρ_s is particle density (2650 kg m^{-3}), ρ_w is the water density (1003 kg m^{-3}) and d_{50} is median grain size (m) (Soulsby, 1997).

The parametrization of the Shields parameter, as improved by Soulsby and Whitehouse (1997), reads:

$$\theta_{cr} = \frac{0.3}{1 + 1.2D_*} + 0.055 \left[1 - \exp(-0.02D_*) \right] \quad (8)$$

270 where D_* is the dimensionless grain size calculated with

$$D_* = \left(\frac{g(\rho_s - \rho_w)}{\nu^2} \right)^{\frac{1}{3}} d_{50}. \quad (9)$$

The strength of this model is its simplicity, but we found it to result in estimates of the critical stress that were an order of magnitude too small compared to values determined in the laboratory from in situ samples (Fig. 4b).

4.2 Thompson et al. (2019)

275 Thompson et al. (2019) developed predictive models for critical shear stress based on physical and biological characteristics in the Celtic Sea and North Sea. Their approach combined principal component analysis (PCA) and multiple linear regression, identifying key predictors such as median grain size, sorting, kurtosis, percentage of fines, bulk density, porosity, chlorophyll *a*, and organic carbon. Two models were proposed:

Model 1 (Celtic Sea): Included both physical and biological parameters, suggesting that bed stability increases with grain size, better sorting, and higher bulk density, while decreasing with higher fines and organic carbon.

Model 2 (North Sea): Relied on physical parameters only, but over-predicted bed strength when applied to Celtic Sea data.

These models demonstrated that physical characteristics dominate bed stability, while biological factors (e.g. chlorophyll *a*) play a secondary role. However, they also highlighted the complexity and co-variation of sediment properties, making broad-scale predictions challenging without site-specific data.

285 These models were not applicable in our study for several reasons. First, we lacked key parameters such as grain sorting and kurtosis, and organic carbon content, which are essential for Model 1. Second, the model had a negative coefficient for dry bulk density despite Figure 3 of Thompson et al. (2019) showing a positive relationship between bulk density and bed stability. This negative coefficient combined with bulk densities being higher in our data compared to the dataset of Thompson et al. (2019), resulted in unphysical values of the critical shear stress. Finally, their models were calibrated for Celtic and North Sea
290 conditions, which differ from our study area in water depth, sediment composition, hydrodynamic forcing, and stress history.

4.3 A non-stationary physical–biological model

We constructed a parsimonious model that couples time-invariant physical factors – median grain size (d_{50} , μm) and dry bulk density (ρ_B , g cm^{-3}) – with a time-varying biological proxy, chlorophyll *a* (ChlA, $\mu\text{g g}^{-1}$). To fit the model we went back to the raw data obtained from the in situ measurements reported by Joensuu et al. (2018, 2020). Since EROMES measurements
295 are not reliable for very coarse sands, samples with $d_{50} > 300 \mu\text{m}$ were excluded.

The model was determined as a three variable least-squares fit using the individual samples from the raw data. In other words, the model predicts critical shear stress as:

$$\tau_{cr} = \beta_0 + \beta_1 d_{50} + \beta_2 \rho_B + \beta_3 \text{ChlA} \quad (10)$$

where τ_{cr} is critical shear stress (N m^{-2}), β_0 is intercept, d_{50} is median grain size (μm), ρ_B is dry bulk density in (g cm^{-3}),
300 and ChlA is chlorophyll *a* ($\mu\text{g g}^{-1}$).

The fit made to each of the classes (Sand, Mud, Mixed sediments) separately had a modest predictive power, but a fit to all the data shows that the model can predict especially the variation between the classes (Table 3, Fig. 5). For the purpose of applying the model to the seabed classes from Sect. 3.1, the variation between classes is the most important property for the model.

305 While physical variables explained most of the variation in τ_{cr} , adding chlorophyll *a* as a variable increased the R^2 by approximately 0.1. We also note that d_{50} and ρ_B were strongly correlated ($R = 0.86$), while ChlA was weakly correlated with the physical variables ($R = 0.10 - 0.34$).

Table 3. The models for the critical shear stress $\tau_{cr} = \beta_0 + \beta_1 d_{50} + \beta_2 \rho_B + \beta_3 \text{ChlA}$ (Eq. 10) based on data from Joensuu et al. (2018, 2020). The fit to data of all types (bold) is the one used in this study.

Sediment type	β_0 ($N m^{-2}$)	β_1 ($N m^{-2} (\mu m)^{-1}$)	β_2 ($N m^{-2} (g cm^{-1})^{-1}$)	β_3 ($N m^{-2} (\mu g g^{-1})^{-1}$)	R^2
All types	-1.027	0.003	0.568	0.028	0.659
Mud	-0.825	0.002	0.450	0.030	0.144
Sand	-3.967	0.004	2.039	0.022	0.286
Mixed sediments	-1.206	0.001	0.734	0.033	0.418

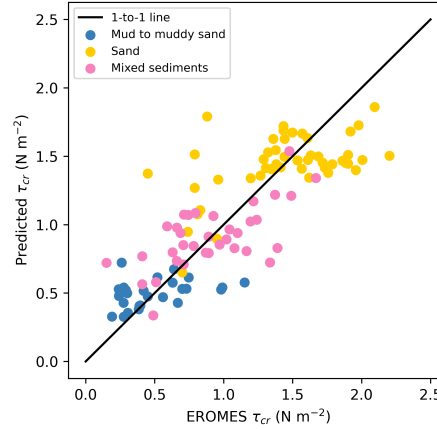


Figure 5. The critical stresses determined with the EROMES device from in situ samples compared to the critical stresses predicted using d_{50} , ρ_B and ChlA (Eq. 10)

Our aim was not to build the most comprehensive model for the τ_{cr} but to define a practical model that can be combined with numerical wave model outputs. To use the modelled critical shear stresses to the spatio-temporal wave model data, we need to determine representative values of d_{50} and ρ_B for each of the three classes (Mud, Sand, and Mixed sediments), and monthly values of ChlA for each of the classes. The model is not applied to coarse sediments or boulders because representative values cannot be reliably determined from the available data.

The raw data from the in situ samples were therefore grouped according to the determined seabed classes: Mud = {ID04, ID16}, Sand = {ID02, ID05, ID06, ID07, ID10, ID11, ID14} and Mixed = {ID01, ID03, ID09, ID15} (see Table 1). For each site, monthly means were computed while retaining the year (e.g. 08-2014 and 08-2015 remain distinct) to avoid overweighting data from the spatial campaign. For d_{50} and ρ_B , class-level monthly means were computed and then averaged to obtain time-invariant values (Table 2). For ChlA , temporal variability was retained by computing monthly means for each class. Months lacking measurements were filled with the off-season mean (September–April).

320 The physical variables (d_{50} and ρ_B) defines the overall magnitude of the critical stress for each class, with Mud being lowest, and Sand being highest (Fig. 4b). The variation caused by the monthly variations in ChlA is significant (Table 4), being up to 52% of the mean value for Mixed sediments, and 29% and 27 % for the Sand and Mud respectively. Nevertheless, the monthly variation never changes the ordering between the classes.

Table 4. The critical stresses $\tau_{cr}(d_{50}, \rho_B, \text{ChlA}(t))$ modelled using the non-stationary physical–biological model (Eq. 10) and the values determined from the data of Joensuu et al. (2018, 2020) (Table 2). $\langle \rangle$ denotes the average of all the monthly values.

Sediment type	$\langle \tau_{cr} \rangle$	$\min(\tau_{cr})$	$\max(\tau_{cr})$
Mud	0.49	0.41	0.55
Sand	1.56	1.31	1.73
Mixed sediments	1.02	0.82	1.35

5 Spatially extensive wave-induced shear stresses

5.1 Numerical model results

325 Modelled shear stresses were estimated based on the near-bottom velocities (Sec. 2.2.1), the representative grain sizes (Sec. 4.3), and the friction coefficients (Sec. 2.3). The shear stresses were determined for every model time step from all available data (2014, 2015 and 2017). The in situ data doesn't contain samples from categories Boulders or Coarse sediments. Therefore, no representative grain sizes could be determined, and wave-induced near-bottom stresses could not be determined. Results are therefore only given for categories Mud, Sand and Mixed sediments, while the other areas are masked out.

330 Mean modelled stresses were generally low, remaining below 1 N m^{-2} across the entire area (Fig. 6a). The 95th percentiles are between 0.5 and 1 N m^{-2} in shallow, exposed areas with large grain sizes (boulders) but remained low (around 0.5 for larger areas, especially where the bottom type was classified as sand, and even exceeding 1 N m^{-2}) near the shoreline for smaller areas (Fig. 6b). Maximum values were concentrated in boulder areas, while the nearshore values stayed below 10 . While the areas with sand bottom are highlighted also in the maximum shear stress values, the highest values (exceeding 2 N m^{-2}) (Fig. 6c and Fig. ??).

335) can be found at mud bottoms. These high values are caused by high near bottom velocities in the exposed area (see Fig. A1). The maximum values indicate that the area around directly south-west of the Tvärminne research station is well sheltered from waves, resulting in very low wave-induced near-bottom shear stresses. The nearest location with notable wave-induced bottom stresses was along the shoreline at longitude $23^\circ 06' - 23^\circ 12'$, where the bottom type consisted of coarse sediments.

340 5.2 Modelled exceedance of Exceedance probabilities for critical values shear stress

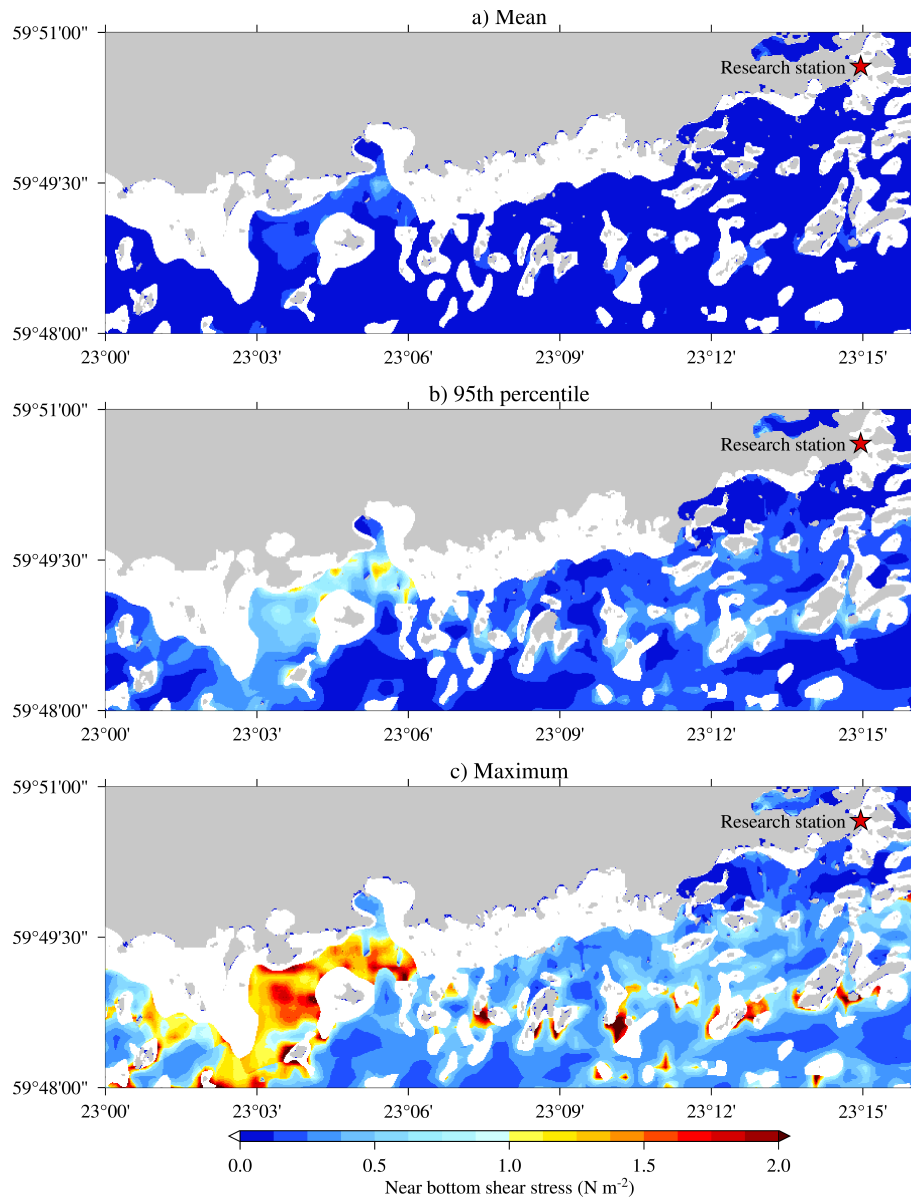


Figure 6. The mean (a), 95th percentile (b), and maximum values (c) of the modelled ~~near-bottom~~ near-bottom shear stress for all the available model data. No results are available for classes Boulders and Coarse sediments (white), since no measurements were available from those classes to determine representative grain sizes. The red star marks the Tvärminne research station for reference.

~~The modelled near-bottom~~ Modelled near-bottom shear stresses were compared to ~~the theoretically derived critical stresses.~~ The exceedance probabilities shown in Fig. 7 indicates the frequency at which critical shear stresses to estimate resuspension

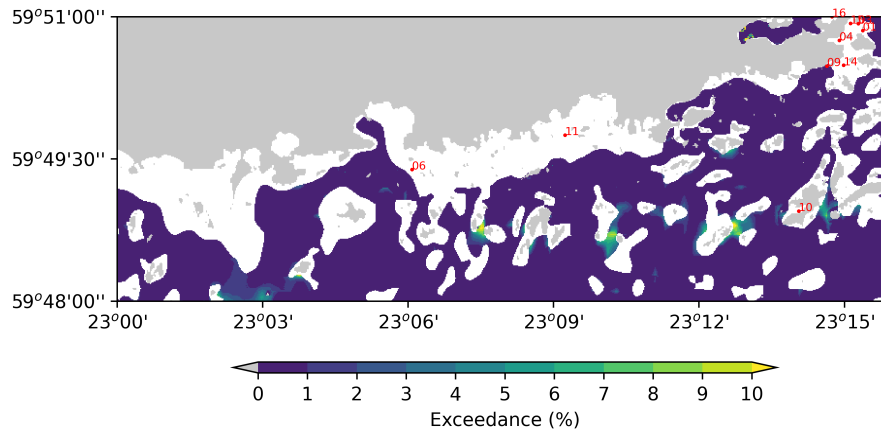


Figure 7. Percent of times the modelled shear stresses exceeded the modelled critical values. No results are available for classes Boulders and Coarse sediments (white), since no measurements were available from those classes to determine representative values for grain size, dry bulk density and chlorophyll *a*.

exceedance probabilities. These probabilities reflect the likelihood that wave-induced water motions could theoretically resuspend sediments.

345 The exceedance probability depends on three main factors: *i*) the shear stress exceeds the critical value, indicating potential sediment resuspension. Exceedance depends on wave conditions, *ii*) the water depth, and *iii*) the bottom type. Several sheltered areas are particularly prone to seabed class. The critical threshold was determined from the model in Sect. 4.3, and therefore varied monthly. Exceedance probabilities were determined simply from the fraction of times the modelled shear stress for a given time exceeded the modelled critical shear stress for the given class and month. The model is not applicable to categories
 350 Boulders and Coarse sediments, and those areas are therefore masked out.

Exceedance of the critical shear stress threshold was generally low across the study area (Fig. 7). Localized patches in the outer archipelago exhibited exceedance of up to 10%, indicating that sediment mobilization mostly occurs during episodic high-energy events. These areas were not limited to the coastline but also appeared among groups of islands and islets located about 2–3 km from the shoreline where the water is shallow, and includes narrow channels that concentrate wave energy.
 355 Sheltered nearshore areas remained below the threshold, suggesting stable sediments and minimal resuspension potential. Even during high-wind events, modeled wave-induced resuspension due to shallow depths (which increase shear stress) and fine sediments (which lower the critical stress). There is therefore not a direct connection between exceedance probability and the near-bottom velocity maps in Appendix B. Shear stresses rarely exceeded predicted or measured thresholds, indicating that sediment mobilization is episodic and limited to localized areas.

360 Kahma (2021) estimated the potential for wave-induced near-bottom velocities using the long-wave (7 s) wave heights from a ray-tracing model as a proxy. The results of Kahma (2021) were 10% exceedance values. While they are able to identify some areas that might be vulnerable to higher wave-induced near-bottom velocities, the author noted that they are not a substitute

for specifically modelling the near-bottom velocities. The use of wave heights as a proxy can naturally also not account for the variation in the seabed type, ~~as done in this study.~~

365 Due to the highly heterogeneous nature of the factors influencing resuspension in the coastal area off Hanko, the resulting exceedance probabilities form a mosaic-like pattern. Notable changes in exceedance values near the shore occur when the bottom type shifts from coarse sediments to sand or mud (Fig. ??), which alters the critical stress, even if wave conditions remain roughly the same. Similar observations were made by Valanko et al. (2010) in the same area, particularly in even shallower regions where waves were the primary driver of resuspension.

370 Exceedance probabilities were generally under 10%, but larger areas showed a resuspension probability ranging from 20 and 50%. These areas were not limited to the coast but also appeared within a group of islands and islets located about 2–3 from the shoreline, where the water is shallow. Exceedance probabilities above 50% were found only in small, isolated regions, and the probability of exceeding 70% was restricted to areas close to the coast or the temporal variation of the critical stress caused by changing biological activity, as done in this study.

375 The fraction of times the modelled shear stresses exceeded the modelled critical values.

5.3 Wave-induced stresses during representative high-wind events

We now present the modelled near bottom shear stresses during high winds blowing from the southerly sector between SW and SSE in late November Two late-November 2015, when sustained wind speeds exceeding 20 m s^{-1} and gusts approaching 26 m s^{-1} were recorded at the FMI Hanko-Russarö automatic weather station ($59^{\circ}46'25.08'' \text{ N } 22^{\circ}56'55.26'' \text{ E}$), 18 km SW from the Tvärminne station. These episodes offer valuable insight into how strong winds trigger wave-induced sediment resuspension in the area.

The significant wave height (a), near-bottom orbital velocities (b) and stresses (c) for 28 November 2015 22 UTC.

385 On 27 and storms illustrate the impact of strong winds on wave forcing and sediment resuspension. On 28 November, southwesterly ($200\text{--}243^{\circ}$) winds of approximately south-westerly winds ($19\text{--}20 \text{ m s}^{-1}$) gradually shifted to a more southerly direction ($165\text{--}171^{\circ}$) by 29 November. Southwesterly winds are common in this region and can generate large waves that propagate into nearshore areas. On 28 November the significant wave height outside the edge of the archipelago was close to generated significant wave heights of ~ 3 , still being around m offshore and ~ 2 inside m within the archipelago (Fig. 8a). The wave height was reduced significantly near the shore, but since the wave-induced near-bottom orbital velocities are also determined by the wave period, they were still in the order of Near-bottom orbital velocities reached 0.5 m s^{-1} for large stretches of the coastline along exposed coastlines (Fig. 8b). The wave-induced shear stress near the bottom was modelled to exceed, producing localized shear stresses exceeding 2 N m^{-2} at some points near the coast (Fig. 8c), which is around the limit for the modelled critical shear stress for coarse sediments (Table ??). The highest values were modelled where the bottom type was Boulders, since the modelled stress depends on the grain size through Eq. 3.

395 The most intense storm in 2015 occurred on the morning of 30 November, when sustained wind speeds event was more severe, with SSE winds of $23\text{--}25 \text{ m s}^{-1}$ were recorded from roughly $150\text{--}160^{\circ}$ (SSE). A peak wind of 26.2 m s^{-1} was

measured at 11:00 local time. Winds from this direction generated waves exceeding 4 m that propagated through the outer archipelago, funneling energy into shallower inshore areas (Fig. 9a). The wave model suggest that in some shallow locations, s^{-1}) causing offshore wave heights beyond 4 m and near-bottom orbital velocities can be close to velocities approaching 1 m s^{-1} in particularly exposed coastal locations shallow exposed areas (Fig. 9b).

The modelled near-bottom shear stress near the coast exceeded 2 N m^{-2} across extensive outer archipelago areas, conditions sufficient to mobilize coarse sediments and cause widespread resuspension (Fig. 9c). Such elevated stresses are capable of resuspending not only fine sediments but also coarser fractions, potentially leading to abrupt increases in turbidity and nutrient fluxes

405 While the highest shear stresses were mostly concentrated to the same areas in both cases, the areas with sand bottom in the western part of the area were more exposed during the SSE winds on 30 November. These two examples represent typical cases of higher waves propagating towards the shore, with south-westerly winds being the most dominant in the area. Together these two events demonstrate that sediment mobilization is highly episodic, concentrated in exposed shallow areas and constricted channels, with implications for turbidity, nutrient fluxes, and benthic habitats.

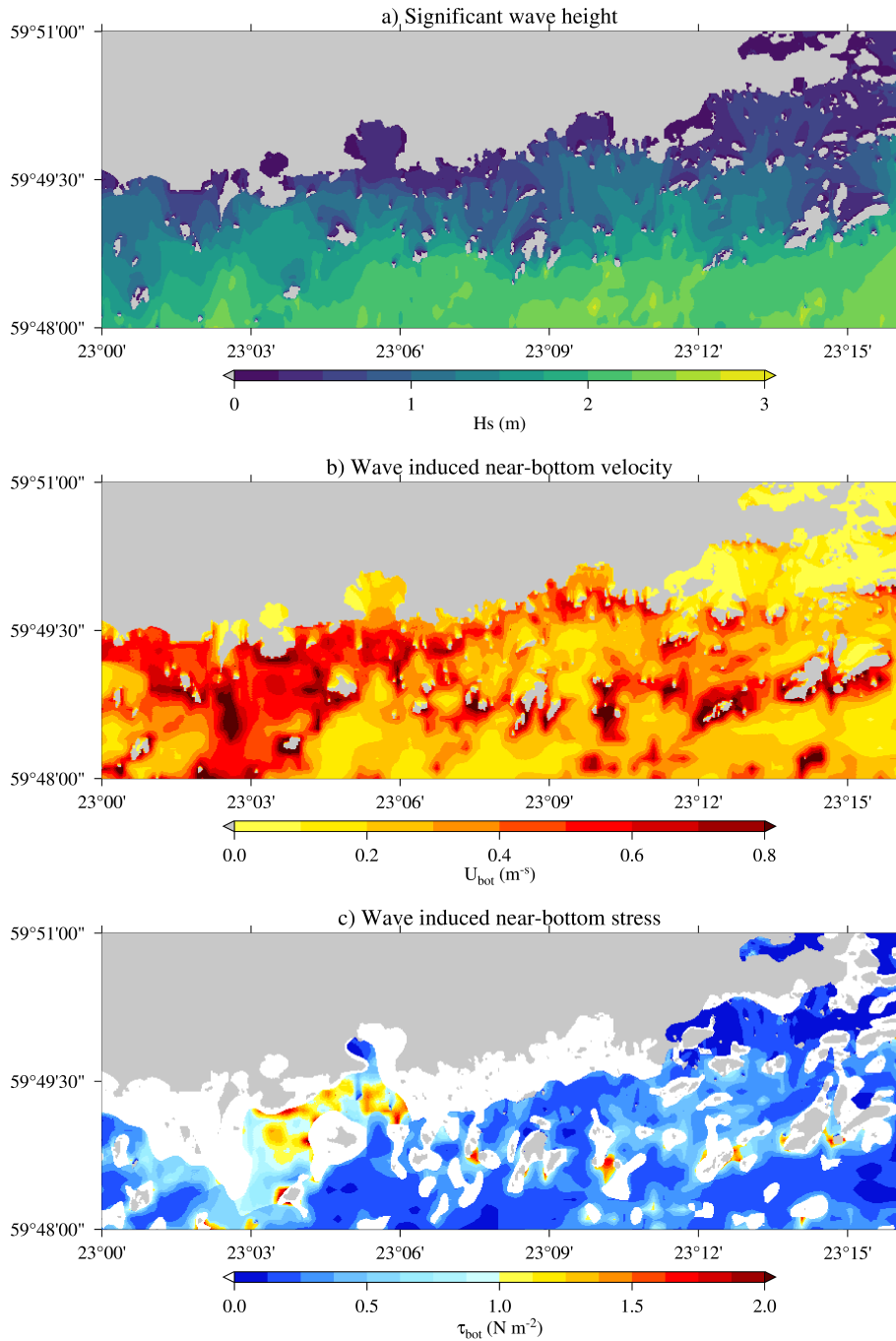


Figure 8. Wave conditions on 28 November 2015 during SW winds: (a) significant wave height, (b) near-bottom orbital velocity, (c) shear stress. Near bottom stresses are not available for classes Boulders and Coarse sediments (white), since no measurements were available from those classes to determine representative grain sizes.

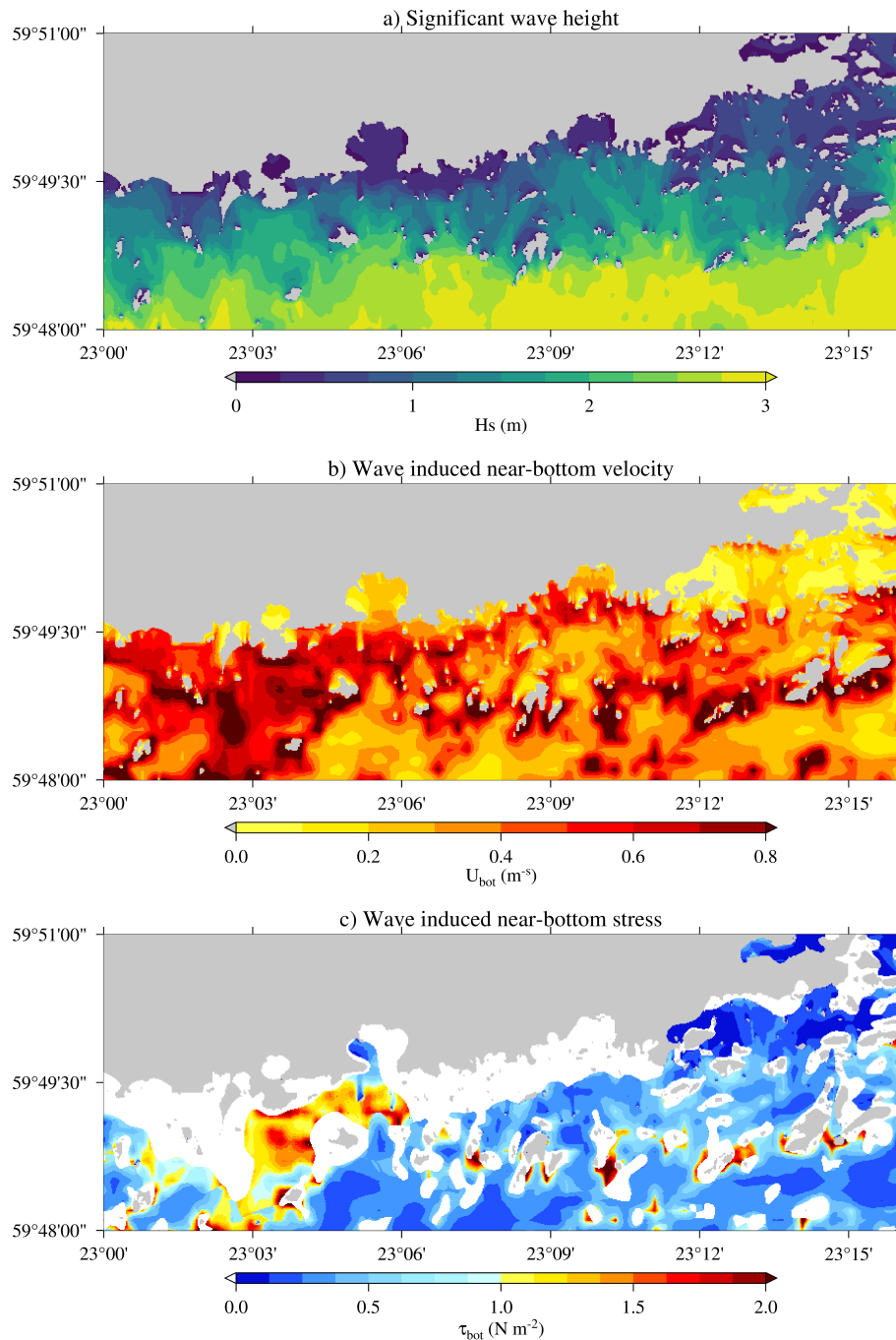


Figure 9. The Wave conditions on 30 November 2015 during SSE winds: (a) significant wave height, (ab) \bar{u} -near-bottom orbital velocities velocity, (bc) and shear stress. Near bottom stresses are not available for classes Boulders and Coarse sediments (e white) for 30 November 2015 10 UTC, since no measurements were available from those classes to determine representative grain sizes.

410 While local bathymetry and island shielding moderate the spatial extent of wave action, shallow areas exposed to the prevailing wind direction remain particularly vulnerable. These observations align with the numerical model findings, which indicate that frequent resuspension events can occur even in sheltered archipelago regions. However, actual resuspension thresholds depend strongly on sediment composition, biological stabilization (

6 Discussion

415 The erodibility of natural sediments is influenced by a complex interplay of physical, geochemical, and biological sediment properties. For example, benthic fauna can modify sediment erodibility by altering water content, bulk density, and the particle size distribution through bioturbation activities (de Deckere et al., 2001; Le Hir et al., 2007). The experimental critical shear stresses used in this study were derived from natural submerged sediment samples, capturing variability across both space (Joensuu et al., 2018) and time (Joensuu et al., 2020). The theoretical grain-size-based thresholds following Soulsby and Whitehouse (1997) 420 underestimated the sediment stability of the data by Joensuu et al. (2018, 2020) by roughly an order of magnitude. Indeed, previous work by e.g. , (biofilms, vegetation), and temporal variations in bulk density — factors that can render real-world resuspension patterns more complex than those predicted by simple grain-size models — Thompson et al. (2019) has shown that bulk density is an important parameter when predicting the critical shear stress, while also incorporating more detailed information about the grain size distribution (e.g. kurtosis).

425 Overall, the November 2015 wind events provide a clear example of how episodic storms can rapidly mobilize coastal sediments in the Baltic Sea's archipelago, with significant implications for water quality and benthic ecosystems.

6.1 Comparison to measured critical stresses

Even though the modelled critical stresses are based on the best available data on wave conditions and bottom type, they do not account for the variability in actual grain sizes, their potential mixed distributions, or other factors, such as biological activity, 430 that could influence resuspension events.

To assess this uncertainty in the model data, we compared the theoretical critical stresses to experimental values obtained in the laboratory from in-situ samples. The experimental critical shear stresses, measured with the EROMES device, were notably higher ($\hat{\tau}_{cr} = 0.45\text{--}1.56\text{ }^{-2}$) compared to the theoretical critical shear stresses derived from modelled grain sizes ($\tau_{cr}(d_{50}) = 0.13\text{--}0.21\text{ }^{-2}$) or from measured grain sizes ($\tau_{cr}(\hat{d}_{50}) = 0.11\text{--}0.28\text{ }^{-2}$) (see Table 1). Our data did not contain detailed information 435 about the grain size distribution, so unfortunately we could not apply the models of Thompson et al. (2019) directly, but we could only assume some typical values for the missing parameters. We still found that the models of Thompson et al. (2019) were not a good description for our data. One of the main issues was that the dependence on the bulk density was negative when using multiple variables, even though the authors had found a positive dependence when using only the bulk density to describe the critical stresses (see their Figure 3). It would seem like the model did not extrapolate well to the higher values 440 of bulk density in our data. This discrepancy in sign for the coefficient might have been caused by correlations between the used variables, but we did not investigate the causes in more detail. Another reason for the weak predictive power of the model

by Thompson et al. (2019) to our data might be the biological activity that can vary strongly with depth, and our data were collected in a much shallower region.

445 The primary limitation of grain-size-only models is their inability to account for consolidation and biological effects. Bulk density is a strong predictor of sediment stability: high-density sediments are more compacted and resistant to erosion, whereas low-density sediments are loose and easily mobilized. Biological activity further modifies stability, especially throughout the growth season, complicating critical shear stress estimates and spatial mapping. We therefore proposed a model that addresses these limitations by incorporating bulk density and chlorophyll *a* as a proxy for biostabilization.

450 These discrepancies indicate that while the modelled critical shear stresses are routinely exceeded, the modelled shear stresses rarely surpass the critical stress values determined by the EROMES device from in situ samples. In fact, at most locations, the measured critical stress is never exceeded. The exception is location ID11, where the modelled shear stresses exceed the measured value of 1.13 ^{-2} (Fig. ??). While the depth and bottom type is similar at both ID06 and ID11, ID06 is clearly more sheltered during strong wave events, as seen in Fig. 8 and 9. More generally, we also modelled shear stresses exceeding 2 ^{-2} in larger areas near the coast during the SSE winds on 30 November 2015. We decided to build our model that 455 relies on a few key variables for two main reasons. First, a model can only be applied if the necessary data is available. Using only three variables increases the likelihood that future datasets will contain all the required variables. Second, many of the variables correlate, and using several correlated variables further increases the uncertainty in the estimates for the individual coefficients when working with a limited data set. We chose to fit our model to three parameters: median grain size, dry bulk density and chlorophyll *a*. The physical aspects are covered by the grain size and bulk density, while the biology is represented 460 by the chlorophyll *a*. There are no objective way to choose the variables, but these three have been used in previous models and it is expected that they might be among the variables that are more routinely measured compare to e.g. grain size distributions.

The three parameter linear model could explain most of the variation of the measured shear stresses between the classes (Mud, Sand, and Mixed sediments) (Fig. 9), which exceeds the theoretical critical shear stress for coarser sediments (Table ??) and the measured critical shear stresses at all measurement locations.

465 The modelled critical stresses — which are based solely on the median grain size — lack biogeochemical factors such as sediment particle size distribution and bulk density, which are central in explaining the critical shear stresses observed in in situ sediment samples (Grabowski et al., 2011; Jepsen et al., 1997).

Distributions of modelled shear stresses at two of the most exposed locations. Here, F represents the cumulative distribution function, with the y -axis on the right indicating the probability of exceedance. The solid and dashed lines correspond to the 470 modelled and measured critical shear stress values, respectively.

The depth (z), median grain size, d_{50} (z), the modelled 95th percentile and maximum stress, τ_w (z), and the critical shear stresses, τ_{cr} (z), at each measurement location (see Fig. 2). Measured values are denoted by a hat (e.g. \hat{d}_{50}). The theoretical critical shear stress has been determined using both the modelled grain size, $\tau_{cr}(d_{50})$, and the measured grain size, $\tau_{cr}(\hat{d}_{50})$.

Site	Depth	Type	(in situ)	d_{50}	\hat{d}_{50}	τ_w^{95th}	τ_w^{max}	$\tau_{cr}(d_{50})$	$\tau_{cr}(\hat{d}_{50})$	$\hat{\tau}_{cr}$
ID01	3.9	Mixed sediment	0.15	0.16	0.03	0.10	0.14	0.14	0.78	
ID02	3.2	Sand	0.34	0.29	0.04	0.29	0.19	0.18	1.16	
ID03	3.0	Mixed sediment	0.15	0.13	0.03	0.17	0.14	0.13	1.12	
ID04	2.3	Mud	0.09	0.06	0.01	0.05	0.13	0.11	0.54	
ID05	2.6	Sand	0.34	0.33	0.04	0.09	0.19	0.19	0.62	
ID06	3.0	Sand	0.34	0.22	0.50	0.54	0.20			

475

0.16 0.81 ID07 3.0 Sand 0.34 0.57 0.05 0.15 0.20 0.28 0.76 ID09 3.0 Mixed sediment 0.15 0.17 0.08 0.19 0.16 0.16 0.95 ID10
3.8 Sand 0.34 0.44 0.17 0.19 0.20 0.23 0.94 ID11 3.2 Sand 0.34 0.26 0.53 1.21 0.20 0.18 1.13 ID14 3.4 Sand 0.34 0.27 0.05
0.14 0.21 0.19 1.56 ID15 3.7 Mixed sediment 0.15 0.15 0.02 0.06 0.15 0.15 0.59 ID16 3.5 Mud 0.09 0.12 0.02 0.06 0.13 0.14
0.45

480

5). Nonetheless, the variation of the individual critical stress measurements from the data within a single class were not explained equally well (Table 3). The model especially struggled with samples from a muddy seafloor, while performing better on samples classified as mixed sediments. Joensuu et al. (2020) found that, compared to the other classes, the shear stress for muddy bottoms were more heavily influenced by the biology, and we surmise that a single variable (ChlA) might not be enough to capture the biological effects well enough to sufficiently model the variations in critical stress on muddy seabeds. Nonetheless, if the aim is to generalize the measurements spatially with only class-based maps, each class can only be represented by a single value. It is therefore most critical that the model can separate the varying behaviour between the classes. It follows, however, that if spatial maps with more detailed information would be available, they would simultaneously increase the requirements on the model for the critical shear stress.

485

490 7 Discussion

Our study highlights that bridging the gap between single in situ measurements and larger scale numerical simulations is far from straightforward. One of the largest uncertainties seems to be the classification of the seabed types and finding representative values for the classes. The combination of our measurements with the EMODnet seabed model had two main weaknesses: 1) Our in situ data could not provide representative values for all of the classes. While areas covered with boulders are not relevant from a resuspension perspective, lacking results of the large areas marked as coarse sediments near the coastline is a clear limitation. 2) The classification doesn't seem to properly match up with the bottom types determined from the in situ samples. Several stations that had been determined as sand from the samples were located in the coarse sediment category in the EMODnet data.

495

The erodibility of natural sediments is influenced by variations in their physical, geochemical, and biological properties. For example, benthic fauna can modify sediment erodibility by altering water content, bulk density, and the particle size distribution through bioturbation activities (de Deckere et al., 2001; Le Hir et al., 2007). The experimental critical shear stresses used in this study were derived from natural submerged sediment samples, which account for the naturally occurring variability over both time (?) and space (?). Nonetheless, the theoretical (modelled) shear stresses were lower than the experimental values by factors ranging from 3.9–8.4 for mixed sediments, 3.3–4.7 for mud, and 2.7–8.2 for sand.

500

Several potential errors could explain the large discrepancies between observed and modelled critical shear stresses. First, the wave model itself might be inaccurate. A second, although probably lesser, source of uncertainty lies in the bottom depth and wave model simulation itself. The water depth used in the wave model directly influences the results, as surface waves are affected by factors like bottom friction and wave breaking, both of which depend on local water depth. More critically, the water depth is essential for transferring surface wave energy to the bottom, as wave motion attenuates rapidly with depth. This

505

510 sensitivity is evident from wave measurements made with the inner wave buoy, where the water depth is approximately 17 metres; if a 15 meter depth is used to transfer the measured surface waves to the seafloor, the mean orbital velocities increase by 26% (not shown). ~~While inaccuracies in water depth of this magnitude are possible, they are insufficient to account for the observed discrepancies (200–700%), and the sensitivity.~~ Nevertheless, the sensitivity to small discrepancies in the water depth should decrease in extremely shallow depths, as horizontal wave motion does not attenuate significantly when the wavelength
515 is at least 20 times the water depth. Furthermore, accurate estimates of near-bottom mean currents were not available for this study, and the absence of current data likely biases the resuspension probabilities toward lower values. Nevertheless, current speeds are expected to be relatively low compared to the maximum wave-induced velocities, especially since tidal currents in the the ~~Baltic~~ Baltic Sea are generally weak.

~~A second potential source of error is the spatial grain size data. These data were only available in broad categories (e.g., sand, coarse sediments), leading to significant uncertainty regarding the actual median grain size at specific locations, particularly for mixed sediments. However, using the measured median grain size in the theoretical calculations (column $\tau_{cr}(\hat{d}_{50})$ in Table 1) did not significantly alter the results at the sample locations. It is important to note, though, that this agreement does not validate the accuracy of the modelled median grain sizes in other areas.~~

~~The third source of discrepancy stems from the reliance on the median grain size alone to model erodability, although e.g. large variations in the grain size distribution might cause armoring effects. There is no consensus on the correct form of the wave friction factor, and our results suggest this was the primary cause of error in our study. This presents a two-fold challenge for modelling sediment resuspension: *i*) how can this effect be parameterized in a practical yet accurate way, and *ii*) is it possible to acquire the necessary data for such parameterization?~~

~~In addition to the actual grain size distribution, it is well known that biota plays a significant role in the erodability of sediments, both directly and indirectly. Directly, it affects bed roughness and structure, while indirectly, it influences bulk density, porosity, and particle size distribution. Bulk density is the mass of sediment per unit volume, including the pore spaces, and it is negatively correlated with erodibility. Sediments with high bulk density are more compacted, making them more resistant to hydrodynamic forcing and requiring higher shear stress to initiate erosion. In contrast, low bulk density sediments are typically loose, unconsolidated, and often freshly deposited. These sediments contain more water and pore space, making them structurally weaker and more susceptible to erosion under relatively low hydrodynamic energy. Although erodability could be described using bulk density – whether or not biota is present – we also know that biological activity varies over time. These temporal fluctuations, such as seasonal changes, induce variations in properties like bulk density, complicating the mapping of seafloor characteristics.~~

~~Our results indicate that Overall, sediment resuspension potential in the study area is highly heterogeneous, even without considering biological factors. These challenges raise questions about the practical applicability of a more complex erodability model, even if an accurate one were available. One possible approach could involve a modified median grain size model, which, while non-physical, could implicitly account for other variations (e.g., bulk density) by increasing the grain size. However, this model would no longer accurately represent the actual grain sizes at the seafloor and would need to be calibrated separately for each area.~~

545 Despite the inherent uncertainties in the forcing data, the modelled near-bottom shear stresses suggest that wind-driven waves can initiate frequent sediment resuspension events, even in more sheltered areas of the archipelago. High-wind events, in particular, may cause significant resuspension, impacting water quality and nutrient cycling. It is likely that the modelled resuspension frequencies are overestimated, with accuracy depending on local sedimentary environments, habitat structure, and benthic biota. Until further studies reduce the uncertainties in modelled critical shear stresses, the exceedance probability maps in the Hanko archipelago. Even with accurate wave forcing simulations, exceedance probabilities should be interpreted more qualitatively than quantitatively. qualitatively until larger datasets and regional calibration reduce uncertainty. Future work should expand empirical measurements, incorporate biological metrics, and test model transferability across regions.

7 Conclusions

555 This study We implemented a numerical spectral wave model (SWAN) with an exceptionally high spatial resolution (20 m) for the coastal archipelago area of Hanko in the Baltic Sea. The near-bottom wave parameters from the wave model Modeled wave-induced shear stresses were combined with median grain sizes (d_{50}) estimated from available spatial data of the seabed type. We also calculated d_{50} -based seabed data to estimate potentials for sediment resuspension and compared against laboratory-derived critical shear stresses and compared them with laboratory values previously determined from in situ samples collected in the area. Finally, we estimated exceedance frequencies based on the hourly model data.

560 The high-resolution wave data revealed that wave-induced Our results reveal a strong spatial variability in near-bottom velocities are highly variable in the complex coastal archipelago of the study area. When combined with the rapidly changing depth and seabed conditions, the modelled shear stresses orbital velocities and sediment resuspension probabilities exhibited extreme heterogeneity.

565 The shear stresses, driven by depth gradients and exposure differences. Nevertheless, theoretical critical shear stresses derived from in situ samples were 3–8 times higher than the theoretical values calculated using d_{50} grain size estimates. These differences were large enough to reduce the resuspension probability from approximately ~15 % to near 0 % at some of the sample stations. The proposed explanation for these significant discrepancies lies in the biogeochemical properties of the sediments. based on grain size alone underestimate sediment stability. To address this limitation, we developed a parsimonious predictive model that integrates grain size, bulk density, and seasonal chlorophyll a as a proxy for biostabilisation. The model was found to be relatively accurate to predict critical shear stresses between sediment classes, and was therefore well suited to be used with the class-based spatial maps available for our study area.

575 In conclusion, Our model could predict a significant seasonal variation in the critical shear stress based on the the seasonal chlorophyll a values, thus highlighting the importance of including the biological activity when modelling the critical shear stress. At the same time it is not obvious how to best model the highly heterogeneous conditions limit the ability to map sediment resuspension potential in complex coastal areas using only in situ samples. The numerical wave model can accurately simulate the highly variable wave conditions, making it useful for studies on carbon cycling or the likelihood of organic matter resuspension. However, our findings suggest that even with highly accurate wave, depth, and seabed data, reliable estimates

of sediment resuspension probabilities cannot be achieved without considering the biological and biogeochemical properties when estimating critical shear stresses effect of the biological activity, especially on a more detailed level than the class based monthly values used in this study. Our findings in comparing our data to previously published models for critical shear stress also suggests that applying these type of locally determined models to other geographical areas might be extremely challenging, if even feasible.

This study underlines the importance of incorporating both physical and biological factors – and their temporal dynamics – into sediment transport models to achieve reliable predictions of erosion thresholds and resuspension potential. Additional work is still required to construct models that can reconcile data from different geographical areas and conditions, and that can accurately predict the observed spatio-temporal variations in critical shear stress both between in within seabed classes. Such improvements would be of significant support to coastal management and ecosystem restoration.

Code and data availability. The seabed data can be accessed through <https://www.emodnet-geology.eu/data-products/seabed-substrates/>. The open source SWAN model can be downloaded at <https://swanmodel.sourceforge.io/>. The wave buoy data is archived in a repository (Björkqvist et al., 2025) and will be opened upon the acceptance of the manuscript. The sediment data from 2014 and 2015 are archived in a repository (Savela, 2025) and will be opened upon the acceptance of the manuscript.

Appendix A: Definition of wave parameters

Third generation numerical wave models model the so called wave spectrum $S(\omega)$ (m^2s), which gives the variance density of waves of different (angular) frequency $\omega = 2\pi f$ (rad s^{-1}) and direction, θ (rad), where f (Hz) is the linear frequency. The variance of a wave component is directly proportional to the square of its height, which is directly proportional to its energy.

The wave model solves the action balance equation, not the energy balance equation, since the spectral variance density is only conserved in deep water without currents. Since this study did not use currents, we give the action balance equation (e.g. Holthuijsen, 2007) below without currents:

$$\frac{\partial N}{\partial t} + \nabla_{\mathbf{x}} \cdot (c_g N) + \frac{\partial c_\sigma N}{\partial \sigma} + \frac{\partial c_\theta N}{\partial \theta} = \frac{G_{tot}}{\sigma}, \quad (\text{A1})$$

where $N = S/\sigma$ is the wave action, c_g is the group speed of a wave component, c_σ and c_θ signifies the speed of the change in frequency and direction, $\nabla_{\mathbf{x}}$ is the spatial partial derivative, and G_{tot} is a sum of the so called source terms, which model the different physical processes that add, remove or redistribute energy of the wave components. Without currents the intrinsic frequency σ (rad s^{-1}) equals the angular frequency ω .

The wave parameters were calculated from the modelled or measured wave spectrum. First, the near-bottom wave spectrum was calculated (The SWAN team, 2024):

$$S_b(\omega) = \frac{S(\omega)}{\sinh^2 kh}, \quad (\text{A2})$$

where $S(\omega)$ (m^2s) is the aforementioned surface wave spectrum, h (m) is the water depth, and k (rad m^{-1}) is the wavenumber solved from wave frequency using linear wave theory. Note, that the wave spectrum from both wave measurements and model output is usually given as a function of f , and in this case $E(f) = 2\pi S(\omega)$ (m^2Hz^{-1}) to conserve the area under the spectral curve (i.e. the total variance of the wave field).

The maximum ~~near-bottom~~near-bottom orbital velocity U_{bot} (m s^{-1}) is defined ~~using the near-bottom~~(The SWAN team, 2024)
using the near-bottom spectrum as

$$U_{bot} = \sqrt{2 \int S_b(\omega) \omega^2 d\omega} = \sqrt{2} U_{rms}, \quad (\text{A3})$$

where U_{rms} is the root-mean-square orbital velocity at the bottom.

615 The ~~near-bottom~~near-bottom amplitude a_{bot} (m) is defined as

$$a_{bot} = \sqrt{2 \int S_b(\omega) d\omega}, \quad (\text{A4})$$

while the ~~near-bottom~~near-bottom mean wave period is defined as

$$T_{m_{bot}} = 2\pi \sqrt{\frac{\int S_b(\omega) d\omega}{\int S_b(\omega) \omega^2 d\omega}} = \sqrt{\frac{\int E_b(f) df}{\int E_b(f) f^2 df}}. \quad (\text{A5})$$

The relationship between these three parameters is therefore

$$620 \quad a_{bot} = \frac{T_{m_{bot}} U_{bot}}{2\pi}, \quad (\text{A6})$$

meaning that two of them exactly determines the third.

Appendix B: Near-bottom velocities, U_{bot}

Figure A1 shows the mean, 95th percentile and max values of the modelled ~~near-bottom~~near-bottom velocities. These velocities are based purely on the wave model data, and don't contain any effects from the chosen grain sizes.

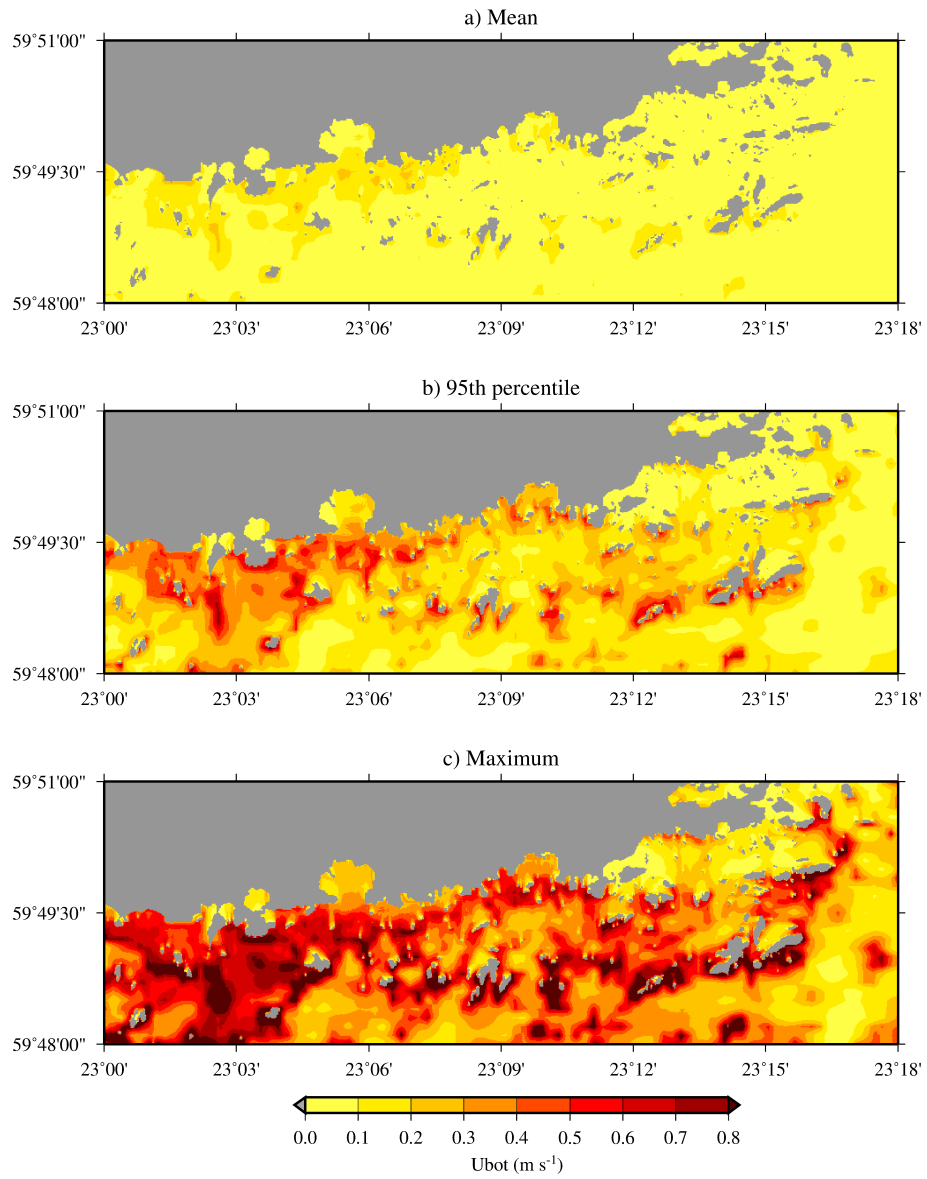


Figure A1. ~~Near-bottom~~ Near-bottom velocities (U_{bot}) as modelled by the SWAN model.

625 *Author contributions.* The study was initiated by MS and AN, and further conceptualized by MS, AN, HP and JVB. Majority of the sediment samples were collected by AN and analyzed by MS. The critical shear stresses from the samples were determined by MS. The wave model simulations were performed by VA and processed by JVB. The theoretical shear stresses were determined by HP and JVB, and the new model for the shear stress was constructed by MS and JVB. The wave measurements were processed by JVB. The manuscript was prepared by JVB and MS with contributions from all authors.

630 *Competing interests.* The authors declare that they have no competing interests.

Acknowledgements. Data used in this publication was made available by the EMODnet Geology project, <http://www.emodnet-geology.eu> funded by the European Commission Directorate General for Maritime Affairs and Fisheries. These data were collected by the Geological Survey of Finland. We thankfully acknowledge the work by [Mr Kimmo Tikka to process the bathymetrical data used to construct the wave model grid and](#) the FMI technical staff in deploying and retrieving the wave buoys. This project got funding from Walter and ~~Andrée~~ [Andrée](#) de Nottbeck Foundation and Onni Talas Foundation (MS). [We are also grateful for two anonymous reviewers for constructive comments that improved the manuscript.](#)

635

References

- Abdolali, A., Roland, A., van der Westhuysen, A., Meixner, J., Chawla, A., Hesser, T. J., Smith, J. M., and Sikiric, M. D.: Large-Scale Hurricane Modeling Using Domain Decomposition Parallelization and Implicit Scheme Implemented in WAVEWATCH III Wave Model, Coastal Engineering, 157, 103–656, <https://doi.org/10.1016/j.coastaleng.2020.103656>, 2020.
- 640 Alari, V. and Raudsepp, U.: Simulation of Wave Damping Near Coast due to Offshore Wind Farms, Journal of Coastal Research, 28, 143–148, <https://doi.org/10.2112/JCOASTRES-D-10-00054.1>, 2012.
- Alenius, P., Myrberg, K., and Nekrasov, A.: The physical oceanography of the Gulf of Finland: a review, Boreal Environ. Res, 3, 97–125, 1998.
- 645 Andersen, T.: Seasonal variation in erodibility of two temperate, microtidal mudflats, Estuarine, Coastal and Shelf Science, 53, 1–12, 2001.
- Andersen, T. J. and Pejrup, M.: Biological Mediation of the Settling Velocity of Bed Material Eroded from an Intertidal Mudflat, the Danish Wadden Sea, Estuarine, Coastal and Shelf Science, 54, 737–745, <https://doi.org/10.1006/ecss.2001.0856>, 2002.
- Andersen, T. J., Lund-Hansen, L. C., Pejrup, M., Jensen, K. T., and Mouritsen, K. N.: Biologically induced differences in erodibility and aggregation of subtidal and intertidal sediments: a possible cause for seasonal changes in sediment deposition, Journal of Marine Systems, 650 55, 123–138, <https://doi.org/10.1016/j.jmarsys.2004.09.004>, 2005.
- Björkqvist, J.-V., Pettersson, H., and Roine, T.: Wave buoy data from the Tvärminne area from 2017, <https://doi.org/10.5281/zenodo.15781282>, 2025.
- Black, K. S., Tolhurst, T. J., Paterson, D. M., and Hagerthey, S. E.: Working with Natural Cohesive Sediments, Journal of Hydraulic Engineering, 128, 2–8, [https://doi.org/10.1061/\(ASCE\)0733-9429\(2002\)128:1\(2\)](https://doi.org/10.1061/(ASCE)0733-9429(2002)128:1(2)), 2002.
- 655 Booij, N., Ris, R., and Holthuijsen, L. H.: A third-generation wave model for coastal regions 1. Model description and validation, Journal of Geophysical Research, 104, 7649–7666, <https://doi.org/10.1029/98jc02622>, 1999.
- Dade, W. B., Nowell, A. R. M., and Jumars, P. A.: Predicting erosion resistance of muds, Marine Geology, 105, 285–297, [https://doi.org/10.1016/0025-3227\(92\)90194-M](https://doi.org/10.1016/0025-3227(92)90194-M), 1992.
- Datawell, BV: Datawell Waverider Manual, https://datawell.nl/wp-content/uploads/2024/09/datawell_manual_dwr4_2024-09-23.pdf, last accessed: 04.11.2025, 2024.
- 660 Datawell, BV: Datawell Waverider Reference Manual, https://datawell.nl/wp-content/uploads/2025/01/datawell_manual_dwr-mk3_dwr-gwr-sg_2025-01-08.pdf, last accessed: 04.11.2025, 2025.
- de Deckere, E. M. G. T., Tolhurst, T. J., and de Brouwer, J. F. C.: Destabilization of Cohesive Intertidal Sediments by Infauna, Estuarine, Coastal and Shelf Science, 53, 665–669, <https://doi.org/10.1006/ecss.2001.0811>, 2001.
- 665 Decho, A. W.: Microbial biofilms in intertidal systems: an overview, Continental Shelf Research, 20, 1257–1273, [https://doi.org/10.1016/S0278-4343\(00\)00022-4](https://doi.org/10.1016/S0278-4343(00)00022-4), 2000.
- Edge, K. J., Dafforn, K. A., Simpson, S. L., Ringwood, A. H., and Johnston, E. L.: Resuspended contaminated sediments cause sublethal stress to oysters: A biomarker differentiates total suspended solids and contaminant effects, Environmental Toxicology and Chemistry, 34, 1345–1353, <https://doi.org/10.1002/etc.2929>, 2015.
- 670 Eerola, K.: Twenty-One Years of Verification from the HIRLAM NWP System, Weather and Forecasting, 28, 270–285, <https://doi.org/10.1175/WAF-D-12-00068.1>, 2013.
- Grabowski, R. C., Droppo, I. G., and Wharton, G.: Erodeability of cohesive sediment: The importance of sediment properties, Earth-Science Reviews, 105, 101–120, <https://doi.org/10.1016/j.earscirev.2011.01.008>, 2011.

- Green, M. O. and Coco, G.: Review of wave-driven sediment resuspension and transport in estuaries, *Reviews of Geophysics*, 52, 77–117, 675 <https://doi.org/10.1002/2013RG000437>, 2014.
- Harris, R. J., Pilditch, C. A., Hewitt, J. E., Lohrer, A. M., Van Colen, C., Townsend, M., and Thrush, S. F.: Biotic interactions influence sediment erodibility on wave-exposed sandflats, *Marine ecology progress series*, 523, 15–30, 2015.
- Heiskanen, A.-S.: Factors governing sedimentation and pelagic nutrient cycles in the northern Baltic Sea, Ph.D. thesis, University of Helsinki, Helsinki, <https://jyu.finna.fi/Record/jykdok.759971>, doctoral dissertation, summary part, 1998.
- 680 Holthuijsen, L. H.: *Waves in Oceanic and Coastal Waters*, Cambridge University Press, Cambridge, <https://doi.org/10.1017/CBO9780511618536>, 2007.
- Jepsen, R., Roberts, J., and Lick, W.: Effects of Bulk Density on Sediment Erosion Rates, *Water, Air, and Soil Pollution*, 99, 21–31, <https://doi.org/10.1023/A:1018355626070>, 1997.
- Joensuu, M., Pilditch, C. A., Harris, R., Hietanen, S., Pettersson, H., and Norkko, A.: Sediment properties, biota, and local habitat structure 685 explain variation in the erodibility of coastal sediments, *Limnology and Oceanography*, 63, 173–186, <https://doi.org/10.1002/lno.10622>, 2018.
- Joensuu, M., Pilditch, C. A., and Norkko, A.: Temporal Variation in Resuspension Potential and Associated Nutrient Dynamics in Shallow Coastal Environments, *Estuaries and Coasts*, 43, 1361–1376, <https://doi.org/10.1007/s12237-020-00726-z>, 2020.
- Kahma, K. K.: Wind-generated long wave climate in the Tvärminne area, *Geophysica*, 56, 29–37, 2021.
- 690 Kaskela, A. M., Kotilainen, A. T., Alanen, U., Cooper, R., Green, S., Guinan, J., van Heteren, S., Kihlman, S., Van Lancker, V., Stevenson, A., and the EMODnet Geology Partners: Picking Up the Pieces—Harmonising and Collating Seabed Substrate Data for European Maritime Areas, *Geosciences*, 9, <https://doi.org/10.3390/geosciences9020084>, 2019.
- Koch, E. W., Ackerman, J. D., Verduin, J., and van Keulen, M.: Fluid Dynamics in Seagrass Ecology—from Molecules to Ecosystems, in: *Seagrasses: Biology, Ecology and Conservation*, Springer, Dordrecht, https://doi.org/10.1007/978-1-4020-2983-7_8, 2007.
- 695 Komar, P. and Miller, M.: The Threshold of Sediment Movement Under Oscillatory Water Waves, *Journal of Sedimentary Petrology*, 43, <https://doi.org/10.1306/74D7290A-2B21-11D7-8648000102C1865D>, 1973.
- Le Hir, P., Monbet, Y., and Orvain, F.: Sediment erodability in sediment transport modelling: Can we account for biota effects?, *Continental Shelf Research*, 27, 1116–1142, <https://doi.org/10.1016/j.csr.2005.11.016>, 2007.
- Madsen, J., Chambers, P., James, W., Koch, E., and Westlake, D.: The interaction between water movement, sediment dynamics and sub- 700 merged macrophytes, *Hydrobiologia*, 444, 71–84, <https://doi.org/10.1023/A:1017520800568>, 2001.
- Michaud, E., Desrosiers, G., Mermillod-Blondin, F., Sundby, B., and Stora, G.: The functional group approach to bioturbation: II. The effects of the *Macoma balthica* community on fluxes of nutrients and dissolved organic carbon across the sediment–water interface, *Journal of Experimental Marine Biology and Ecology*, 337, 178–189, 2006.
- Miettunen, E.: Circulation and transport dynamics in the Archipelago Sea, Ph.D. thesis, University of Helsinki, <http://hdl.handle.net/10138/587710>, 2024. 705
- Mulsow, S., Boudreau, B. P., and Smith, J. A.: Bioturbation and porosity gradients, *Limnology and Oceanography*, 43, 1–9, 1998.
- Pascolo, S., Petti, M., and Bosa, S.: On the Wave Bottom Shear Stress in Shallow Depths: The Role of Wave Period and Bed Roughness, *Water*, 10, 1348, <https://doi.org/10.3390/w10101348>, 2018.
- Pettersson, H., Kahma, K. K., and Tuomi, L.: Wave Directions in a Narrow Bay, *Journal of Physical Oceanography*, 40, 155–169, 710 <https://doi.org/10.1175/2009JPO4220.1>, 2010.

- Roberts, J., Jepsen, R., Gotthard, D., and Lick, W.: Effects of Particle Size and Bulk Density on Erosion of Quartz Particles, *Journal of Hydraulic Engineering*, 124, 1261–1267, [https://doi.org/10.1061/\(ASCE\)0733-9429\(1998\)124:12\(1261\)](https://doi.org/10.1061/(ASCE)0733-9429(1998)124:12(1261)), 1998.
- Savela, M.: Hydrological and Sediment Dataset from the Tvärminne Coastal Area (2014–2015), Dataset, <https://doi.org/10.5281/zenodo.15796802>, 2025.
- 715 Schünemann, M. and Köhl, H.: A device for erosion measurements on naturally formed, muddy sediments: the EROMES-System, Tech. rep., GKSS Research Centre, 1991.
- Shields, A.: Anwendung der Ähnlichkeitsmechanik und der Turbulenzforschung auf die Geschiebebewegung, Preußische Versuchsanstalt für Wasserbau, Berlin, Germany, english translation available at: <http://authors.library.caltech.edu/25992/1/Sheilds.pdf>, 1936.
- Soulsby, R.: Dynamics of Marine Sands, Thomas Telford Publishing, London, UK, 1997.
- 720 Soulsby, R. L. and Whitehouse, R. J. S.: Threshold of Sediment Motion in Coastal Environments, Conference paper, <https://doi.org/10.3316/informit.929741720399033>, 1997.
- The SWAN team: SWAN scientific and technical documentation, Tech. rep., Delft University of Technology, <http://swanmodel.sourceforge.net/download/zip/swantech.pdf>, downloaded on 06.01.2026, 2024.
- Thompson, C. E. L., Williams, M. E., Amoudry, L., Hull, T., Reynolds, S., Panton, A., and Fones, G. R.: Benthic controls of resuspension in UK shelf seas: Implications for resuspension frequency, *Continental Shelf Research*, 185, 3–15, <https://doi.org/10.1016/j.csr.2017.12.005>, 2019.
- 725 Valanko, S.: Dispersal and metacommunity dynamics in a soft-sediment benthic system: how well is the seafloor connected?, 2012.
- Valanko, S., Norkko, A., and Norkko, J.: Strategies of post-larval dispersal in non-tidal soft-sediment communities, *Journal of Experimental Marine Biology and Ecology*, 384, 51–60, <https://doi.org/10.1016/j.jembe.2009.12.012>, 2010.
- 730 Westerlund, A., Tuomi, L., Alenius, P., Miettunen, E., and Vankevich, R. E.: Attributing mean circulation patterns to physical phenomena in the Gulf of Finland, *Oceanologia*, 60, 16–31, <https://doi.org/10.1016/j.oceano.2017.05.003>, 2018.
- Zhang, G., Hu, S., Yu, X., Zhang, H., and Gong, W.: Physical drivers and parameter sensitivities of pearl river-derived sediment dispersal on the Northern South China Sea Shelf: a modeling study, *Ocean Science*, 21, 2041–2068, <https://doi.org/10.5194/os-21-2041-2025>, 2025.